Available online at www.sciencedirect.com

Manufacturing Letters

Manufacturing Letters 41 (2024) 568–574

52nd SME North American Manufacturing Research Conference (NAMRC 52, 2024)

Mechanical Property Improvements of LPBF-AlSi10Mg via Forging to Modify Microstructure and Defect Characteristics

Austin Ngo[a*], Noah Kohlhorst[b], Svitlana Fialkova[c], Bradley Jared[d], Tony Schmitz[d], Glenn Daehn[b], Jennifer L.W. Carter[a], Jian Cao[e], John J Lewandowski[a*]

[a]*Case Western Reserve University (CWRU), 10900 Euclid Ave, Cleveland, OH 44106, USA*
[b]*The Ohio State University (OSU), 281 W Lane Ave, Columbus, OH 43210, USA*

[c]*North Carolina Agricultural and Technical State University (NCA&T), 1601 E Market St, Greensboro, NC 27411, USA*

[d]*University of Tennessee, Knoxville (UTK), TN 37996, USA*

[e]*Northwestern University (NU), 633 Clark St, Evanston, IL 60208*

* Corresponding authors. *E-mail address:* jjl3@case.edu, aqn5@case.edu

Abstract

Additive Manufacturing (AM) processes have versatile capabilities but are susceptible to the formation of as-cast non-equilibrium microstructures, process-induced defects, and porosity, which have deleterious effects on the mechanical performance. As part of our NSF-ERC-HAMMER program, isothermal forging was investigated as a novel post-processing technique for refining microstructure, reducing process defect severity, and thereby improving mechanical properties. Specimens of Laser Powderbed Fusion (LPBF) AlSi10Mg were fabricated over a range of process parameters and tensile tested as a baseline. Initial work focused on duplicate AM material that was then hot forged with 20% strain to investigate the effects of isothermal forging at one temperature and strain rate on the microstructure, tensile, and fatigue properties of the as-deposited materials. The microstructures, process-induced defect populations, and tensile/fatigue properties of both as-deposited and forged materials were quantified and analysed by OM, EBSD, XCT, and SEM by various NSF-ERC-HAMMER team members. Isothermal hot forging was found to induce recrystallisation and modify process-induced defect geometry along with increasing tensile ductility. The effects of AM deposition parameters and forge post-processing conditions on LPBF AlSi10Mg will be discussed in terms of microstructure, mechanical properties, and fractography.

Peer-review under responsibility of the scientific committee of the NAMRI/SME.
Keywords: Laser Powderbed Fusion; Forging; AlSi10Mg; Defects; Hybrid manufacturing processes

1. Introduction

While AM processing provides significant design and topology options, the resulting as-deposited AM material/product typically exhibits non-equilibrium microstructures and process-induced defects that can significantly impact mechanical performance and reliability [1-3] as well as both location- and orientation-dependent properties [4-9]. The as-deposited/cast AM microstructure may exhibit significant texture, columnar grains, etc. depending on the type of AM process (e.g., LPBF, EBPBF, DED, WAAM, etc.) and details of process parameters utilized (e.g. powder bed preheat, scan strategy, laser power, laser scan velocity, hatch spacing, etc.). AM process-induced defects include anomalies of various types that include Keyhole, Lack of Fusion (LoF), Balling, and solidification porosity [10]. While post-processing

Peer-review under responsibility of the scientific committee of the NAMRI/SME.

heat treatments and/or HIP can be used to impart some microstructural changes and the potential of defect modification/closure, remnants of the as-deposited structure (including defects) may remain and thereby compromise the resulting properties.

A recent review [1] summarized the inferior fatigue properties in AM-processed materials compared to wrought and cast materials and concluded that process-induced defects and as-deposited surface roughness were primary contributors to the poor fatigue performance [1]. Recent fatigue studies on LPBF-processed Ti-6Al-4V focused on characterizing process-induced defect have confirmed the importance of these factors [2,3]. Dzugan *et al.* documented both location- and orientation-dependent properties via the use of miniaturized samples across a number of AM-processed alloys [4-7]. While HIP can be used to reduce/eliminate porosity [1,4,8,9], the microstructural changes that accompany such high temperature exposures during HIP may also produce unacceptable reductions in strength [1] that offset the improvements from reduced porosity [4,8,9].

Recent developments in hybrid manufacturing processes provide opportunities to address such issues on as-deposited materials containing process-induced defects with the use of local/global incremental deformation to modify microstructure and eliminate process defects [11]. Such processes would use open die forging/deformation with robotic manipulation for flexible on-demand manufacturing in contrast to the much higher forces required in closed-die forging used in repetitive mass-production [12-13].

The NSF-ERC-HAMMER team (https://hammer.osu.edu/) [14] is exploring various hybrid autonomous manufacturing approaches to significantly improve the performance and reliability of components manufactured by forging, casting, AM, etc. across various sectors. This preliminary work illustrates the beneficial effects of post-process forging to 20% strain on both the microstructure and tensile properties of LPBF AlSi10Mg. In particular, the paper compares the forging response of material purposely processed to contain LoF defects with material processed to contain minimal defects.

2. Experimental Methods

2.1. Baseline AM build

Builds for mechanical test specimens were fabricated at Youngstown State University on a 3D Systems ProX 320 DMP with a 500W IPG fiber laser with a spot size of 100µm. The feedstock was virgin AlSi10Mg powder with a size distribution of 15-45 µm. Rectangular and hexagonal blanks were built with the long axis resting on the build plate (the horizontal (XY) orientation), perpendicular to the vertical (Z) build direction, as shown in Figure 1. Two build parameter sets (Table 1) were evaluated for this paper–A nominal set with minimal defects (Build A), and a poorly optimized set with large AM process-induced defects and high defect number density (Build D). Other builds (i.e., Builds B and C) examine different process parameters and are the subject of a larger paper. All machined specimens received the same heat treatment procedure recommended by AM industry collaborators–stress relief furnace treatment according to SR1 in ASTM F3318-18, followed by Hot Isostatic Pressing (HIP), and lastly T6 solutionizing and aging (Table 2). After heat treatment, test specimens for tensile testing (ASTM E8-16), uniaxial fatigue (ASTM E466-15), and bend fatigue (ASTM E647-15) were machined to their final dimensions.

Table 1. AlSi10Mg AM build details.

Build ID	Laser Power (W)	Scan Velocity (mm/s)	Defect type	Relative Density (%)
A	370	110	Nominal, minimal defects	99.6
D	370	180	Many small-medium defects	92.2

Table 2. Post-build treatments.

Heat Treatment	Temperature (°C)	Time (min)	Pressure (MPa)
Stress Relief	285	120	Ambient
HIP	510	135	102
T6 (solutionizing)	530	360	Ambient
T6 (aging)	160	360	Ambient

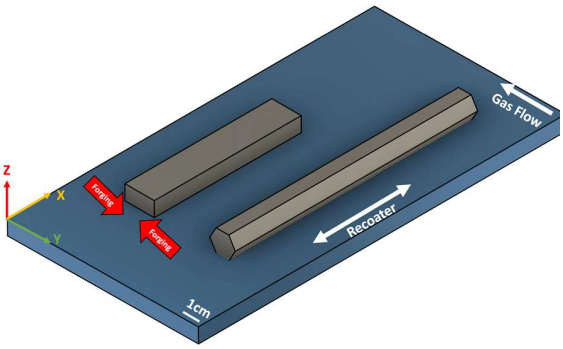

Fig. 1. Schematic of test specimen builds relative to the ProX 320 build plate. Hexagonal rods, built to sit flatly on the build plate, were machined into cylindrical specimens (ASTM E8-16, ASTM E466-15). The forging direction used for the bend bar samples is also shown.

2.2. Isothermal forging

In addition to evaluating the baseline material discussed in Section 2.1 (i.e., 0% forging), duplicate bend bar samples were subjected to post-process isothermal forging with 20% reduction, Figure 1, using an MTS servo-hydraulic press with furnace attachment, as shown in Figure 2. Isothermal forging of additional bend fatigue specimens, which had received the same heat treatment procedure as the baseline specimens, was accomplished by first holding at 530 ºC/1 hour, followed by forged by uniaxial forging to a 20% height reduction in the Y-orientation (Fig. 1) at a strain rate of 10^{-3}/s, followed by a cold water quench. While the stress relief and HIP procedures were not repeated after forging, the forged specimens were then given the same T6 heat treatment to enable comparison with the baseline (i.e., 0% forging) specimens. After T6 heat treatment, tensile specimens were machined from the forged

samples with the tensile axis parallel to the X-direction in Figure 1.

Fig. 2. MTS servo-hydraulic press with furnace chamber for isothermal hot forging. Specimens were compressed on a single axis.

2.3. XCT scanning

Prior to the 20% reduction, Build A and Build D bend fatigue specimens were scanned at NCA&T using X-ray computed tomography (XCT) on a Phoenix Nanotom M, with up to 0.5µm voxel resolution. Analysis of specimens after forging and mechanical testing is ongoing.

2.4. Mechanical Testing

Uniaxial tensile testing was conducted at CWRU under ambient temperature and humidity, in a high alignment fixture and MTS contact extensometer (12.7 mm gauge length) (see Fig. 3). Tests were conducted with a strain rate of 10^{-3}/s with the tensile axis along the X-direction, Figure 1.

Uniaxial high cycle fatigue (HCF) testing following ASTM E466-15 on 0% reduction (i.e., baseline) specimens was conducted on an Instron servo-hydraulic test frame with a load ratio of $R = 0.1$ and cyclic frequency $f = 20Hz$, shown in Figure 4. Fatigue samples were also oriented along the X-direction, Figure 1, and were tested up to a runout limit of $N_f = 10^6$ cycles, with specimen failure defined as catastrophic failure. Several of the heavily defected (i.e., Build D) test specimens failed upon initial setup loading, which was recorded as $N_f = 1$ cycle. A goal of 3 tests per peak stress level was set, though testing of the heavily defected Build D deviated from this goal due to poor, erratic fatigue performance caused by the intentionally produced process-induced defects.

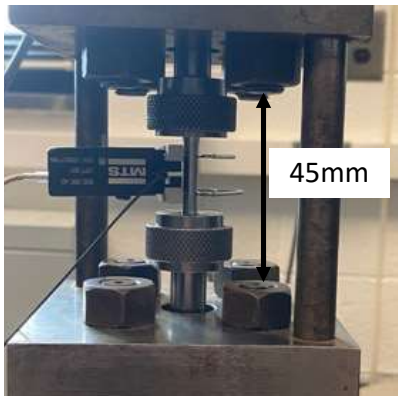

Fig. 3. High-alignment tensile testing setup, with MTS contact extensometer attached to the specimen gauge length.

Fig. 4. Servo-hydraulic test frame and grip setup for uniaxial HCF tests.

2.5. Failure Analysis

Fracture surfaces of all failed tension and fatigue specimens were imaged with optical microscopy (OM) and scanning electron microscopy (SEM) at CWRU. Features such as AM process defects and fatigue crack initiation sites were evaluated in the context of different builds and forging, and the cross-sectional area of tensile specimen fracture surfaces was measured to determine the final reduction in area (RA%).

2.6. Microstructural Analysis

Metallography of test specimens was conducted at OSU. Specimens were prepared for OM to measure defect size, and SEM+EBSD was conducted to characterize grain structure of the baseline (i.e., 0% forging) and after forging to 20% reduction.

3. Results

3.1. XCT scanning

A 3D reconstruction of XCT results on the baseline (i.e., 0% forging) is shown in Figure 5 for both Builds A and D, with each analyzed specimen volume covering approximately 6000 mm^3. Defects are colored corresponding to their volume. Build A (Fig. 5a) contains few defects and is >99% fully dense. The majority of process-induced defects are below 0.01 mm^3 and are concentrated toward the center of the specimen volume. Build D (Fig. 5b), while still >90% fully dense, contains a relatively large amount of LoF defects distributed throughout the entire specimen volume, and defect volumes are an order of

magnitude greater than in Build A–Note the difference in scale in defect volume between specimens.

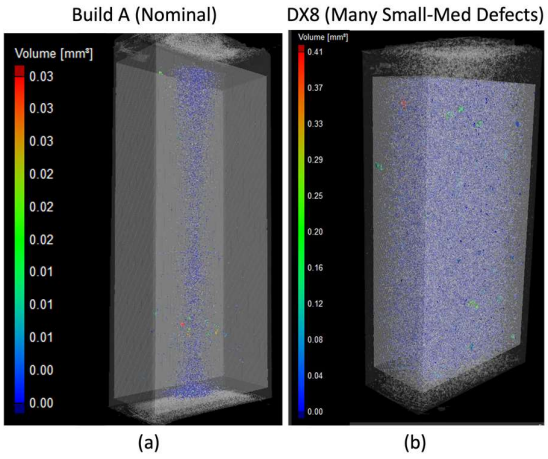

Fig. 5. XCT Scanning of baseline AM builds, with internal process-induced defects colored. (a) Build A, relative density: 99.6%. (b) Build D, relative density: 92.2%.

3.2. Tensile testing

Figure 6 reports yield strength (YS), ultimate tensile strength (UTS), and reduction in area (RA%) as comparative measurements of strength and ductility in Builds A and D under both 0% and 20% forging reduction conditions. Multiple tests were conducted for the baseline 0% reduction condition, with average properties reported and error bars representing standard deviation.

At the baseline 0% reduction, Build D suffers a 30% reduction in UTS compared to Build A due to the severity of its process-induced defects. YS is not reported for Build D because these test specimens failed during elastic deformation, below the limit where the standard 0.2% offset strain could be determined. This lack of plasticity is further reflected when comparing reduction in area, where Build A's RA% is one (1) order of magnitude greater than that of Build D.

Figure 7 shows the extent of defects on the 0% reduction tensile specimen fracture surfaces. No notable process-induced defects appear on the fracture surface of Build A (Fig. 7a), and the fracture surface indicates ductile fracture. In contrast, many lack-of-fusion (LOF) defects, hundreds of micrometers in dimension, appear in Build D (Fig. 7b). Individual feedstock powder particles entrapped in the LOF defect voids can also be seen under high magnification in Fig. 7b, further suggesting the extent of incomplete melting under Build D process conditions.

The 20% forging reduction produced little effect on YS and UTS in Build A (Fig. 6) that contained few defects. While the UTS of Build D does not exceed the average value of the baseline (i.e. not forged) Build D, the UTS of the forged material exceeded that of the lowest performing Build D baseline material. Notably, the 20% forging reduction produces significant increases in RA% for both Builds A and D. In Build A, RA% more than doubles, from 7% to 15%. A 7x increase is seen in Build D, from 0.7% to 5%. The modification of process-induced defects from the 20% forging reduction can be observed from Build D fracture surfaces, as shown in Figure 8. LOF defects have not been eliminated, and powder particles are visible, similar to the baseline 0% forged specimens (Fig 7b). However, the shape of process defects has become more ellipsoidal, reflecting the effect of 20% forging reduction along a single axis.

3.3. HCF testing

HCF test results are reported in *S-N* form in Figure 9. All tests of Builds A and D failed before runout at the given test stress levels. Fatigue tests of the nominal Build A showed consistent *S-N* results at the three peak stress levels which were explored (i.e., 230, 210, and 190 MPa), with three tests at each stress level. Build D showed very poor fatigue performance. Multiple test specimens failed before the full cyclic test loads could be applied, prohibiting evaluation of Build D at the same stress levels as Build A. *S-N* curve behavior was obtained for Build D at stress levels approximately 40% lower than in Build A. Even at these stress levels, N_f is lower and test scatter greater than in Build A, confirming that much lower stresses are required to reach fatigue lifetimes similar to Build A.

3.4. Microstructure

Figure 10 reports the defect area fraction measured using OM at OSU for Builds A and D under both 0% and 20% forging reduction conditions. In the baseline (i.e., 0% forging)

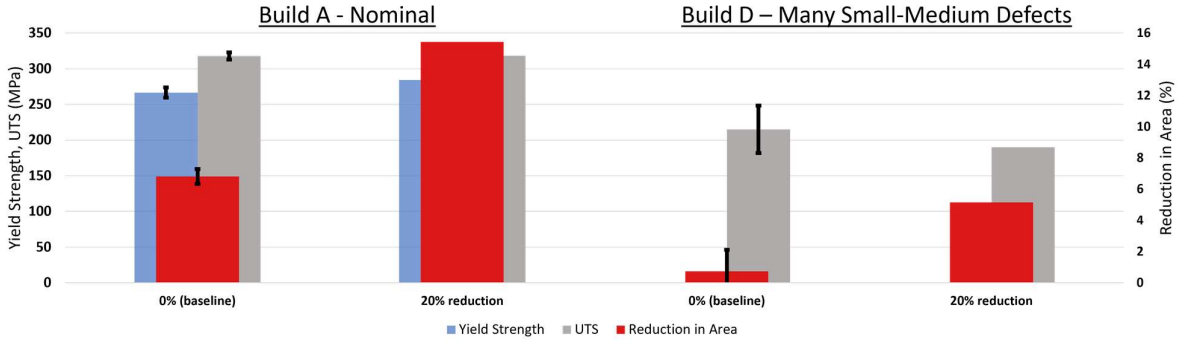

Fig. 6. Mechanical properties determined by tensile testing of AM AlSi10Mg under different build and forging conditions. Error bars on baseline represent ±1 standard deviation.

specimens, the defect area fraction is two (2) orders of magnitude greater in Build D than in Build A. The defect area fraction decreases after 20% forging reduction for both Builds A and D by approximately 50%.

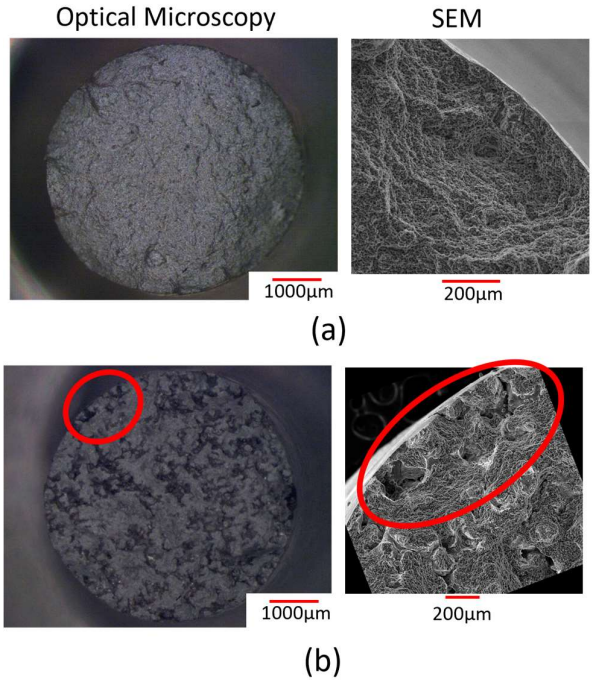

Fig. 7. OM and SEM fractography of (a) Nominal Build A, where no process defects are observed on the fracture surface, and (b) Build D, where large, networking LOF defects cover the entire fracture surface.

Etched microstructures of Builds A and D are shown in Figure 11. Prior to any forging reduction (Figs. 11a, 11c), grain structures exhibit the overlapping "fish-scale" shapes typical in layered AM fabrication. The microstructure of the 20% forged material (Figs. 11b, 11d) consists of smaller, equiaxed grains. These characteristics were confirmed by EBSD mapping, shown in Figure 12. Average grain size was measured from the EBSD maps, also shown in Figure 12, which shows that the average grain size is reduced after 20% forging reduction. The scatter and anisotropy in grain size is also reduced.

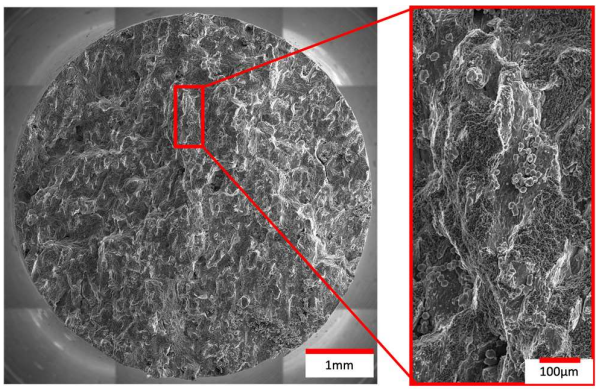

Fig. 8. Composite SEM of Build D tensile specimen fracture surface after 20% forging reduction.

4. Discussion

Consistent with much work in literature [1, 4-9], the tensile properties of LPBF-processed AlSi10Mg, and other alloys, are highly dependent on process conditions as well as subsequent post-processing (i.e., heat treatment, HIP). While the baseline Build A material exhibited properties comparable to other reports of AlSi10Mg processed in the optimal/process window regime [1], the defected Build D samples exhibited essentially zero ductility and failed at the UTS without appreciable yielding despite receiving a HIP treatment. Both XCT and fracture surface analyses in Figs. 5 & 7 showed minimal defects in the Build A material, while Build D showed extensive defects despite the HIP process. This likely results from the potential connected path of sub-surface defects to the sample surface, thereby preventing pore closure during HIP, although entrapped gas may also have contributed.

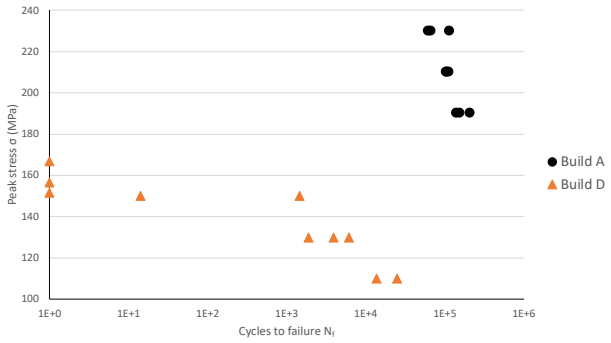

Fig. 9. *S-N* fatigue plot comparing 0% forging (baseline) Build A and Build D tests, with runout limit set at 10^6 cycles.

Significant changes to the tensile properties after 20% forging reduction were obtained for both Builds A and D, with associated changes to both the microstructure and fracture surface details. While neither the yield nor UTS were significantly affected in Build A (Fig. 6), Fig. 12 shows changes to both grain size and texture from the coarser and somewhat columnar as-deposited Build A microstructure to

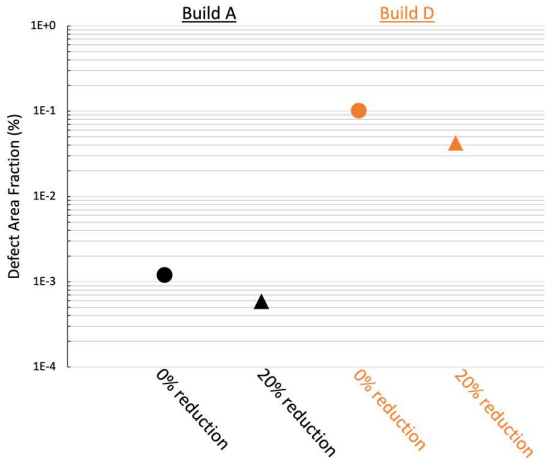

Fig. 10. AM process-induced defect area fraction measured on metallography specimens under different AM build and forging conditions.

that of the 20% forged material that exhibited a reduction in grain size beyond the 20% reduction utilized, suggesting that some amount of recrystallization was imparted. This is consistent with the isothermal forging conditions ($T = 530^{\circ}C, \epsilon = 0.20, \dot{\epsilon} = 10^{-3}/s$) utilized as they were selected based on the conditions likely to produce microstructure refinement based on a large database of Aluminum alloys [15]. The present work utilized 20% reduction to impart some change while ongoing work [16] is exploring higher levels of reduction (e.g. 60%) that shows more significant changes in both microstructure and tensile properties.

While the microstructure refinement at 20% reduction is demonstrated, there were also significant improvements to the Build A ductility/RA%, predominantly in the non-uniform strain, a result of the hot working of the as-deposited Build A microstructure. More impressive are the effects on the heavily defected Build D forged with 20% reduction. While similar microstructure refinement was obtained as that exhibited by Build A, this level of forging reduction was not sufficient to completely close/heal the LoF defects as illustrated by the metallographic cross-sections (Fig. 11) and fracture surface images (Fig. 8) that similarly show LoF defects on the fracture surface. However, even this limited amount of hot working has significantly increased the ductility/RA% with changes to defect dimensions visible in both the metallographic samples as well as fracture surfaces. Ongoing work on identical materials forged to 60% reduction under the same conditions shows further improvements in both the uniform and non-uniform strain, along with both metallographic and XCT examinations showing pore/void collapse and more significant changes to the defect dimensions [16]. It is expected that forging reductions greater than 20% reduction should induce further recrystallization and grain refinement, in addition to further deformation of process-induced voids/defects into elongated defect features. Such modifications should further improve mechanical properties to approach, and even exceed, those exhibited by non-defected material (i.e., Build A). Ongoing work [16] on the effects of larger forging reductions (e.g. up to 60%) will be reported elsewhere, as it is not yet clear what the optimum conditions will be. The optimum conditions will also depend on the desired properties.

It is important to note that the tensile properties after forging were evaluated perpendicular to the forging direction. The mechanical properties will likely become more anisotropic after uniaxial forging due to the changes in microstructure and defect dimensions, but such work provides an opportunity to optimize both the forging conditions (e.g. reduction amount, orientation, etc.) to produce desired performance in different locations of an AM-processed (or cast, etc.) product. However, other recent work has also explored the concept of using AM deposits/material as a forging preform with excellent results [17, 18]. The NSF-ERC-HAMMER team is pursuing this concept for a range of materials and structures (e.g. AlSi10Mg, 316L, etc.) for a variety of AM processes (PBF, DED, WAAM) and expects similar improvements to both microstructure and mechanical performance. The concept of post-process incremental forging may reduce the need for HIP and/or other techniques due to the beneficial aspects of deformation processing on both the microstructure and defect characteristics.

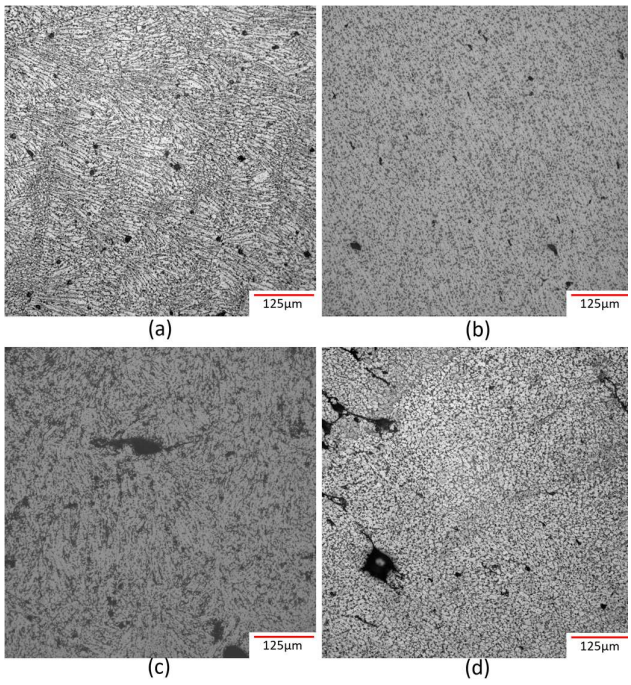

Fig. 11. Polished and etched microstructures of Build A specimens under (a) 0% forging reduction, and (b) 20% forging reduction, compared to Build D specimens under (c) 0% forging reduction, and (d) 20% forging reduction. The non-forged microstructures in (a, c) exhibit a range of grain sizes and orientations as a result of rapid melting and solidification in AM processing, which become more uniformly equiaxed after forging (b, d).

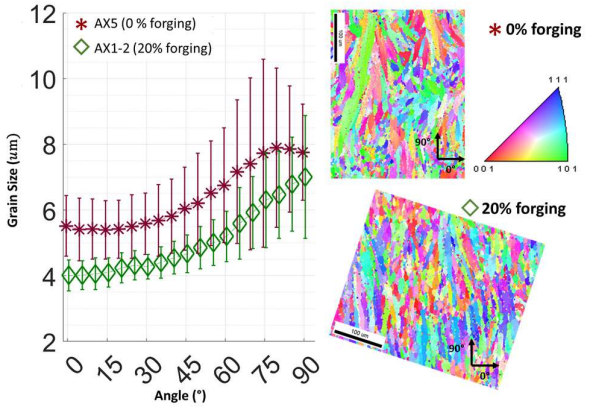

Fig. 12. EBSD mapping and measurement of average grain size in Build A specimens under 0% and 20% forging reduction conditions. Changes in grain size relative to map orientation indicate grain anisotropy.

Conclusions

The NSF-ERC-HAMMER team is exploring the novel use of post-AM process forging on the resulting microstructure, defect characteristics, and tensile properties of LPBF-AlSi10Mg. Preliminary results obtained on both nominally defect-free (i.e., Build A) and heavily defected material (i.e.,

Build D) show significant improvements to the microstructure and tensile properties after 20% reduction. More significant changes are expected with 60% reduction, which is currently under investigation. In particular:

1. The as-deposited, HIP and heat treated nominally defect-free material, Build A, exhibited microstructure and tensile properties/fractography consistent with other results from the literature. The heavily defected material, Build D, exhibited essentially zero ductility/RA along with fracture surface evidence of AM-processed defects, despite the post-process HIP treatment applied.
2. Isothermal hot forging at 530C to 20% reduction in the build direction produced changes to the as-deposited microstructure along with reduction in grain size for both Builds A and D.
3. While the yield and UTS were similar pre- and post-forging for the nominally defect-free Build A, significant (2.5x) increases in the non-uniform strain and RA% were recorded due to the beneficial effects of hot deformation processing.
4. While forging to 20% reduction did not significantly change the UTS of Build D, significant (7x) increases to the ductility/RA% were obtained, with increases to both the uniform and non-uniform strain. SEM analysis revealed changes to the defect dimensions as did the metallographic cross sections.
5. These preliminary findings will inform the development of multiple projects investigating the use of novel post-processing, including forging, to produce materials/structures with tailored location- and orientation-dependent properties.

Acknowledgements

Initial work on the baseline material was supported by America Makes (Project 3012) while the effects of post-process forging study was partially supported initially by the Arthur P. Armington Professorship (Lewandowski). The authors would like to acknowledge support for the bulk of the post-process forging work from the NSF Engineering Research Center for Hybrid Autonomous Manufacturing Moving from Evolution to Revolution (ERC - HAMMER) under Award Number EEC-2133630.

References

[1] Lewandowski, J.J., Seifi, M. Metal additive manufacturing: A review of mechanical properties. *Annual Review of Materials Research* 46, 2016. p. 151–186. https://doi.org/10.1146/annurev-matsci-070115-032024

[2] Narra, S.P., Rollett, A.D., Ngo, A.N., Scannapieco, D., Shahabi, M., Reddy, T., Pauza, J., Taylor, H., Gobert, C., Diewald, E., Dugast, F.X., To, A., Wicker, R., Beuth, J., and Lewandowski, J.J. Process Qualification of Laser Powder Bed Fusion Based on Processing-Defect Structure-Fatigue Properties in Ti-6Al-4V. *Journal of Materials Processing Technology*. 2023. https://doi.org/10.1016/j.jmatprotec.2022.117775

[3] Miner, J.P., Ngo, A., Gobert, C., Reddy, T., Lewandowski, J.J., Rollett, A.D., Beuth, J., and Narra, S.P. Quantifying the Impact of Sparse Lack-of-Fusion Porosity from Melt Track Geometry Variability on Fatigue Life in Powder Bed Fusion - Laser Beam Manufactured Ti-6Al-4V. *Additive Manufacturing* 2023. Pre-print. Manuscript No. ADDMA-D-23-04447.

[4] Dzugan, J., Seifi, M., Rund, M., Podany, P., Grylls, R., and Lewandowski, J.J. The Use of Miniature Specimens to Determine Local Properties and Fracture Behavior of LPBF-Processed Inconel 718 in as-Deposited and Post-Treated States. *Materials*, 15(13), 4724. 2022. https://doi.org/10.3390/ma15134724

[5] Mertova, K., Dzugan, J., Roudnicka, M., Daniel, M., Vojtech, D., Seifi, M., and Lewandowski, J.J. Build Size and Orientation Influence on Mechanical Properties of Powder Bed Fusion Deposited Titanium Parts. *Metals*, 2020; 10(10), doi:10.3390/met10101340.

[6] Pehlivan, E., Roudnicka, M., Dzugan, J., Kralik, V., Dalibor, D., Daniel, M., Seifi, M., and Lewandowski, J.J. Effects of Build Orientation and Sample Geometry on the Mechanical Response of CP-Ti Grade 2 Wire Samples Manufactured by Selective Laser Melting, *Additive Manufacturing*, 2020; 35, 101403. https://doi.org/10.1016/j.addma.2020.101403.

[7] Dzugan, J., Seifi, M., Prochazka, R., Rund, M., Podany, P., Konopik, P., and Lewandowski, J.J. Effects of Thickness and Orientation on the Small-Scale Fracture Behaviour of AM Ti-6Al-4V. *Matls. Charact*., 2018; 143, pp. 94-109. https://doi.org/10.1016/j.matchar.2018.04.003.

[8] Dzugan, J., Seifi, M., Rzepa, S., Prochaska, R., Rund, M., Podany, P., and Lewandowski, J.J. Mechanical Properties Characterization of Metallic Components Produced by Additive Manufacturing Using Miniaturized Specimens. *Virtual and Physical Prototyping*, 2023; 18(1), 2161400.

[9] Dzugan, J., Seifi, M., Rzepa, S., Rund, M., Koukolikova, M., Viehrig, H-W, Liu, Z.H., and Lewandowski, J.J. The Effects of Post-processing on the Local Fracture Toughness Properties of Electron Beam Powder Bed Fusion Ti-6Al-4V Alloy. *Engineering Fracture Mechanics*, 2022; 273, 108697.

[10] Gordon, J. v., Narra, S. P., Cunningham, R. W., Liu, H., Chen, H., Suter, R. M., Beuth, J. L., & Rollett, A. D. Defect structure process maps for laser powder bed fusion additive manufacturing. *Additive Manufacturing*, 2020; *36*, 101552. https://doi.org/10.1016/j.addma.2020.101552

[11] The Minerals, Metals & Materials Society (TMS), *Metamorphic Manufacturing: Shaping the Future of On-Demand Components* (Pittsburgh, PA: TMS, 2019). Electronic copies available at www.tms.org/metamorphicmanufacturing.

[12] Groche, P., Fritsche, D., Tekkaya, E. A., Allwood, J. M., Hirt, G. and Neugebauer, R. Incremental Bulk Metal Forming. CIRP Ann. 2007; 56, 635–656.

[13] Yang, D. Y., Bambach, M., Cao, J., Duflou, J. R., Groche, P., Kuboki, T., Sterzing, A., Tekkaya, A. E. and Lee, C. W. Flexibility in Metal Forming. *CIRP Ann.* 2018; 67, 743–765.

[14] Daehn, G.S., Cao, J., Lewandowski, J. *et al*. Introducing NSF's Hammer Engineering Research Center: Hybrid Autonomous Manufacturing Moving from Evolution to Revolution (Hammer). *JOM* 75, 2023; p. 971–974. https://doi.org/10.1007/s11837-023-05765-y

[15] Prasad, Y.V.R.K., Rao, K.P., Sasidhara, S. Hot Working Guide: A Compendium of Processing Maps. 2nd Ed. Materials Park, OH: ASM International. 2015.

[16] Ngo, A., Kohlhorst, N., Fialkova, S., Jared, B., Schmitz, T., Daehn, G., Carter, J., Cao, J., Lewandowski, J.J. Influence of Post-Process Forging on Microstructure and Properties of LPBF AlSi10Mg. Manuscript in preparation. 2024.

[17] Semiatin, S.L., Kobryn, P.A., Roush, E.D. et al. Plastic flow and microstructure evolution during thermomechanical processing of laser-deposited Ti-6Al-4V preforms. *Metall Mater Trans A* 32, 2001; 1801–1811. https://doi.org/10.1007/s11661-001-0156-0

[18] Furrer, D.U., Heinritz, E., and Boyer, R.R. Laser Deposited Titanium for Forging Preforms. Ladish Co., Inc., Cudahy, WI. Unpublished research, 2000.